



# Challenges for geodetic VLBI in the southern hemisphere

Lucia Plank<sup>a,\*</sup>, Jim E.J. Lovell<sup>a</sup>, Stanislav S. Shabala<sup>a</sup>, Johannes Böhm<sup>b</sup>, Oleg Titov<sup>c</sup>

<sup>a</sup> University of Tasmania, Private Bag 37, 7001 Hobart, Australia

<sup>b</sup> Technische Universität Wien, Gußhausstraße 27-29, 1040 Vienna, Austria

<sup>c</sup> Geoscience Australia, GPO Box 378, Canberra ACT2601, Australia

Received 19 November 2014; received in revised form 17 April 2015; accepted 17 April 2015

Available online 27 April 2015

## Abstract

Inhomogeneous networks and reference frames are an important issue for Very Long Baseline Interferometry (VLBI). In this work we examine the performance of southern stations and baselines in routine VLBI experiments. A positive impact on baseline length repeatabilities of the increased observing effort by the Australian AuScope VLBI antennas is found by analysing three years of global rapid-turnaround VLBI sessions: while worse results are found for southern baselines compared to northern baselines for the first half of the investigated sessions, the northern and southern baseline length repeatabilities are about the same in the second half of the period. In simulations, the actual observing plan with a significantly lower number of observations for southern stations is identified as a major reason for the worse length WRMS for southern baselines, though other factors seem to influence the results as well. Simulating radio source position uncertainties, effects of up to 10 mm are found on baseline length WRMS for long southern baselines. Improving all source position uncertainties through more frequent observations to better than 50  $\mu\text{s}$  could reduce this effect by up to 30%.  
© 2015 COSPAR. Published by Elsevier Ltd. All rights reserved.

**Keywords:** VLBI; Southern hemisphere reference frames; Source uncertainties; IVS; AuScope

## 1. Introduction

Very Long Baseline Interferometry (VLBI) is a space geodetic technique measuring the emission from extragalactic radio sources with globally distributed radio antennas. Global observations are coordinated by the International VLBI Service for Geodesy and Astrometry (IVS; Schuh and Behrend, 2012) and made freely available to the public (e.g. at <http://ivscc.gsfc.nasa.gov>). Positions of the observed radio sources make up the International Celestial Reference Frame (ICRF2; Ma et al., 2009), the most precise quasi-inertial reference frame. Besides that, VLBI is uniquely capable of fully determining the Earth's orientation in space in terms of the Earth orientation parameters (EOPs). Together with the Global

Navigation Satellite Systems (GNSS), Satellite Laser Ranging (SLR), and Doppler Orbitography and Radiopositioning Integrated by Satellite (DORIS), VLBI is used to establish the geodetic coordinate system on Earth, the International Terrestrial Reference Frame (ITRF2008; Altamimi et al., 2011).

The ideal network of VLBI antennas would be homogeneously distributed around the globe and observe continuously, 24 h a day, 7 days a week (24/7). In practice, the northern hemisphere dominates in both landmass and countries capable of contributing to radio astronomy research by funding dedicated observatories. As a consequence, there is a highly unequal distribution of VLBI radio telescopes contributing to the IVS. The lack of radio telescopes also causes an uneven distribution of radio sources in the ICRF, in both the number of sources as well as their nominal uncertainties (Ma et al., 2009). In short, the ICRF2 is more sparse and less accurate in the south.

\* Corresponding author. Tel.: +61 3 6226 2450.

E-mail address: [Lucia.Plank@utas.edu.au](mailto:Lucia.Plank@utas.edu.au) (L. Plank).

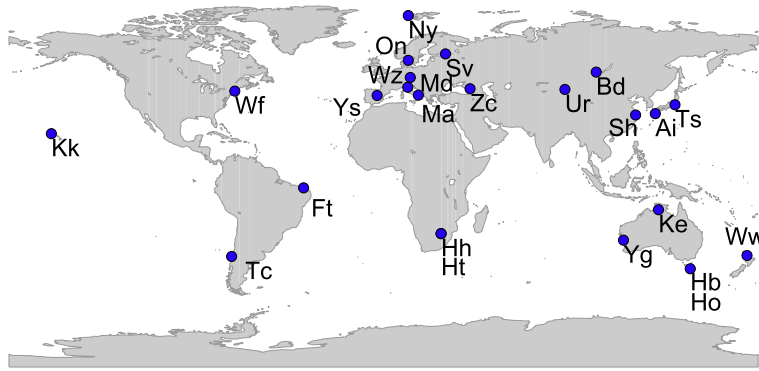


Fig. 1. Map of stations participating in the 2012–2014 R1 and R4 sessions.

Irregular antenna availability, e.g. due to shared facilities with astronomical observing or operational and budget constraints, does not allow for full 24/7 observing and causes the observing network to change from session to session.

The Australian AuScope VLBI array (Lovell et al., 2013) was built in order to tackle these issues, i.e. to (a) increase the number of stations and observations in the southern hemisphere and (b) strengthen the celestial reference frame in the south. An improvement in positions of southern stations through an increase of observations is expected (station position uncertainties scale with the inverse square root of the number of observations). On the other hand, it is not clear in what way southern stations and baselines will profit from a better southern hemisphere CRF. Previous studies confirmed that erroneous source positions can affect other geodetic results like estimated EOPs (MacMillan and Ma, 2007; Nilsson et al., 2012). In an analysis of VLBI data until 2006, Titov (2007) showed that the selection of reference radio sources can have a significant effect on VLBI station positions. This effect is increased for isolated stations (e.g. in the southern hemisphere) and stations with a very low number of observations (e.g. due to low antenna slew speeds).

In this work we investigate the performance of southern hemisphere VLBI stations due to a lower number of observations as well as due to observing sources with less accurate astrometry than their northern counterparts. In Section 2 the motivation of this study is provided by analysis of three years of standard geodetic VLBI observational data. We use simulations to investigate the influence of the observation schedule on geodetic parameters in Section 3, in particular focusing on the difference between northern and southern hemispheres. Our findings are summarised in Section 4.

## 2. VLBI analysis

IVS rapid-turnaround sessions (R1, R4) are undertaken twice a week. Using a fairly stable network of about 7–11 antennas, the data are shipped, correlated and analysed usually within two weeks of the experiment. The timeliness

of the data, but also the high cadence and hence large amount of observations, make the IVS R-sessions a strong contributor to the standard VLBI products, such as the EOPs, TRF, and CRF.

### 2.1. The data

In our investigation, we analysed three years of rapid sessions from 2012 to 2014.<sup>1</sup> Excluding stations that only observed in 1–2 sessions, we find a total of 24 stations observing 463 sources in 302 rapid sessions. As can be seen in Fig. 1, 9 stations are in the southern hemisphere whereas the other 15 in the northern hemisphere. Despite this clear imbalance, for each session the participating stations are distributed as uniformly as possible. On average, 5 northern stations and 4 southern stations contributed to each R-session. In Table 1 the stations are listed in order of increasing latitude (from south to north), showing the number of sessions in which each station took part as well as the median number of scans and observations per session. While a scan is defined as several antennas observing the same source, when more than two antennas observe the identical source at the same time, in one scan one antenna can have several observations with other antennas. When observing in global networks, at each observation epoch the antennas are usually divided in sub-nets, each of them observing one common source. For  $a$  antennas observing the same source, the number of observations (or baselines  $b$ ) in this scan usually is  $b = a(a - 1)/2$ . The process of how these sub-nets are chosen, as well as the selection of target sources and observation epochs is commonly referred to as *scheduling*. Scheduling is a complex procedure including a number of optimisation processes, e.g. described in Petrov et al. (2009) or Sun et al. (2014). Besides basic geometrical issues, the number of scans per station is mainly influenced by the antenna capabilities in terms of sensitivity and slewing speed. One can generally say that larger antennas are much more sensitive than small antennas, however they usually need more time for slewing

<sup>1</sup> At the time of writing, not all data for 2014 were available.

Table 1

Statistics of stations, number of sessions (sess), and median number of scans and observations (obs) per session of the 2012–2014 R1 and R4 sessions. Stations are ordered with increasing latitude, from south to north. In brackets, the size of the dish is given for each antenna. For both hemispheres, we also calculated the median numbers for northern and southern antennas. Besides the numbers for all sessions, we compare the statistics for the first (2012–2013/6) and the second half (2013/7–2014) of the investigated period.

Station (dish)	2012–2014			2012–2013/6			2013/7–2014		
	sess	scans	obs	sess	scans	obs	sess	scans	obs
Hb (12 m)	151	224	415	58	189	336	93	234	461
Ho (26 m)	10	175	341	10	175	341	–	–	–
Tc (6 m)	224	128	221	147	131	223	77	117	220
Ww (12 m)	23	157	341	11	129	177	12	166	373
Yg (12 m)	135	219	430	45	183	292	90	226	491
Hh (26 m)	59	190	399	38	192	409	21	187	383
Ht (15 m)	66	265	572	5	137	344	61	270	575
Ke (12 m)	142	243	473	53	223	391	89	244	544
Ft (14 m)	244	152	313	120	153	313	124	150	311
South	135	190	399	45	175	336	83	207	422
Kk (20 m)	220	243	547	116	245	540	104	240	550
Sh (25 m)	21	378	1021	10	380	1097	11	347	919
Ai (10 m)	20	174	444	–	–	–	20	174	444
Ts (32 m)	122	440	1003	72	420	943	50	483	1158
Ys (40 m)	83	299	984	43	305	1052	40	286	900
Ma (20 m)	99	257	635	59	265	640	40	248	625
Wf (18 m)	91	312	762	49	312	780	42	312	698
Ur (25 m)	13	265	766	5	291	899	8	265	725
Zc (32 m)	68	280	849	33	295	952	35	270	816
Mc (32 m)	37	275	855	24	276	998	13	262	777
Wz (20 m)	278	328	845	155	330	860	123	314	833
Bd (32 m)	70	264	819	32	290	932	38	255	729
On (20 m)	59	326	1084	35	341	1111	24	294	1082
Sv (32 m)	57	301	1032	33	314	1142	24	269	835
Ny (20 m)	269	313	856	141	333	890	128	297	813
North	70	299	849	39	309	938	38	270	813

from one source to the next. The actual on-source time is then proportional to the combined sensitivity of both antennas of a baseline observation.

Scheduling of the IVS R1 and R4 sessions is done using the software SKED [Gipson, 2012](#). While the scheduling process itself requires experience, steady research and adaptations to changing conditions like variable antenna networks, this is not the topic of our investigation. In this paper we rather concentrate on the output of this process and how an increased observing effort of the Australian VLBI antennas positively influenced the results.

As a last comment on this topic it shall be mentioned that the numbers given in [Table 1](#) refer to the observations that were actually used in the analysis. Due to bad observations or antenna failures, these can differ from the originally scheduled number of observations.

The first thing clearly evident in [Table 1](#) is the fact that southern stations have much less scans than the northern ones, namely 190 versus 299 in median scans per station per session. This is likely due to the fact that many of the southern stations are of smaller dish size and hence need longer on-source times to reach a certain level of signal to noise ratio. The second number we give is the median number of observations per station per session. We again find a significant difference between stations of the two hemispheres, with 849 observations for northern stations

and 399 observations for southern stations. While part of it is a direct result of the lower number of scans for the southern stations, another reason could be the lack of suitable partner stations for common baselines in the more sparsely populated southern hemisphere. It is well known (e.g. [Schuh and Böhm, 2013](#); [Petrachenko et al., 2009](#)) that a high number of scans per station helps to better resolve the troposphere and minimise its error on the observations and that a high number of observables improves the station position accuracy. As a consequence, stations with lower numbers of scans and observations might have worse results.

The Australian AuScope VLBI array ([Lovell et al., 2013](#)) consists of three 12 m radio telescopes in Hobart (Hb), Katherine (Ke), and Yarragadee (Yg). Constructed in the year 2010, once all telescopes were properly set up and regularly delivered good results AuScope has contributed to the R1 and R4 sessions on a regular basis with one or two antennas. In mid 2013 operational funding allowed to increase this observing effort to full participation of all three telescopes. In addition new southern antennas were built in Warkworth (Ww, 12 m) and Hartebeesthoek (Ht, 15 m), also supporting the IVS R observing program. In order to investigate the effect of the increased efforts of these new antennas, we compare two time periods: one from the start of 2012 until June

30, 2013 and the other from July 1 until the most recent available session of December 22, 2014. The first period corresponds to the previously standard IVS rapid sessions, while the second period includes more intensive AuScope participation. As a first effect of the new stations we find an increase in the mean total number of stations from 8 in 2012–2013/6 to 9 in 2013/7–2014. With the additional southern stations, in mean we now find 4 southern and 5 northern stations per session compared to a ratio of 3 and 5 respectively for 2012–2013/6.

Comparing the two time periods, we find that while the average number of both scans and observations decreased by about 13% for northern stations, it increased by 18% and 25% in scans and observations respectively for the southern ones. In Fig. 2 we give the number of observations for each of the southern stations and compare the two time periods before/after mid-2013. Additionally we distinguish between observations to other southern stations and those to northern stations. Except of the 15 m antenna in Hartebeesthoek (Ht), we find that the additional observations for sessions after mid-2013 are predominantly to stations in the south while the number of observations to northern antennas did not change significantly. This is shown graphically in Fig. 2. One reason for this could be that with more fast antennas in the southern hemisphere observing together, additional common scans could be added to the schedule while the larger and slower antennas are slewing.

In Table 2 we give the statistics of the observed sources in the two sets of sessions, before and after mid-2013. Hereby the sources are binned by declination into four regions. We find that most of the observed sources are in

Table 2

Statistics of observed sources and number of observations to these sources for the 2012–2014 R1 and R4 sessions. We compare sessions before and after mid-2013 and bin the sources into four regions by declination.

	$[-90^\circ, -40^\circ]$	$[-40^\circ, 0^\circ]$	$[0^\circ, 40^\circ]$	$[40^\circ, 90^\circ]$
<i>2012–2013/6 (156 sessions)</i>				
Sources	45	108	179	68
Observations	20,053	72,221	148,167	176,959
Obs. per session	129	463	950	1134
<i>2013/7–2014 (146 sessions)</i>				
Sources	58	116	199	78
Observations	32,997	93,092	146,099	155,315
Obs. per session	226	638	1001	1064

the northern sky, at declinations between  $0^\circ$  and  $40^\circ$ . The majority of observations per session is found for sources even further north, at declinations above  $40^\circ$ . Overall, the distribution of observations is highly imbalanced, with only 22%/29% of all observations to southern sources, for the two sets of sessions respectively. It is also visible that with the new schedules after mid 2013 the number of observations to southern sources has significantly increased, from about 590 observations per session to about 870.

## 2.2. Analysis of observational data

Starting from the pre-processed data files in NGS-format, as provided by the IVS, the analysis of the above set of 302 sessions was performed using the Vienna VLBI Software (VieVS; Böhm et al., 2012). We applied standard analysis settings, estimating one set of station coordinates, EOPs, and source coordinates per session. The VieTRF13 (Krásná et al., 2014) was used as an a priori terrestrial reference frame for station positions and linear velocities. Station corrections were applied in accordance with the IERS Conventions 2010 (Petit and Luzum, 2010), additionally correcting for tidal and non-tidal atmosphere loading, as provided by the Vienna University of Technology (Wijaya et al., 2013). Antenna coordinates were then estimated by applying a no-net-rotation (NNR) and a no-net-translation (NNT) condition on all stations. Source coordinates were also estimated, applying an NNR condition on the ICRF2 defining sources (Ma et al., 2009). Clocks were modeled as piecewise linear offsets every 60 min with one rate and one quadratic term per clock. Relative constraints of 1.3 cm after 60 min were used. For the troposphere, zenith wet delays were estimated every 60 min with 1.5 cm constraints and gradients were estimated every 6 h using constraints of 0.5 mm. For the weighting of the observations we used the inverse of the sum of squared formal uncertainties as given in the NGS files and, as these tend to be too optimistic, added a further noise floor of  $1 \text{ cm}^2$ .

We compare results in terms of the weighted root mean square (WRMS) of the baseline lengths, called baseline length repeatabilities in the following. The WRMS was

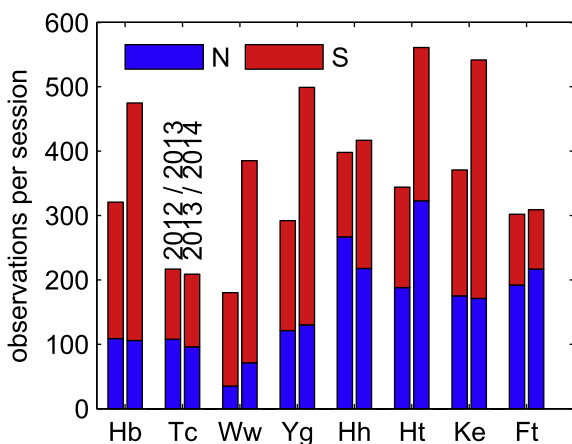


Fig. 2. Median number of observations per session for the southern stations. We distinguish between observations to other stations on the southern hemisphere (red) and those to northern stations (blue). This is done for the two time periods, 2012–2013/6 (left bars) and 2013/7–2014 (right bars). Stations are ordered, from left to right, with increasing latitude. As Hobart26 (Ho) did not observe in any R1/R4 session since mid-2013, this station was omitted here. For the AuScope stations as well as for Ht and Ww, a clear increase in south–south observations is found for the later sessions. (For interpretation of the references to colour in this figure legend, the reader is referred to the web version of this article.)

calculated using the session-wise estimated residual baseline lengths, which are the offsets to the a priori modelled baselines for the individual times of the observations. Hence, long-term station motions due to plate tectonics or tidal displacements were considered in the analysis and are not part of the baseline length repeatabilities. Only baseline estimates within  $\pm 10$  cm of the a priori value were included and baselines with less than five sessions in an investigated time period were eliminated from the statistics. To compare the two hemispheres, the baselines are split into southern baselines (SS) between two southern stations, northern baselines (NN) and mixed (NS) baselines between a station in the southern hemisphere and one in the northern hemisphere.

Baseline length repeatabilities are a standard quality measure of geodetic VLBI data (MacMillan and Ma, 1994; Titov, 2009), independent of the underlying reference frame. As most of the new southern stations are not yet included in the most recent ITRF (ITRF2008; Altamimi et al., 2011) we chose this method rather than, for example, station positions. Baseline repeatabilities usually scale with the length of the baseline. In order to compare different sets of baselines or solutions, we performed a quadratic fit to the sets of SS and NN baselines and compare the WRMS for three baseline lengths, 2000 km, 6000 km, and 10,000 km (Table 3). For the NS baselines, a linear fit was done.

In Table 3 the repeatabilities are shown for the three sets of baselines, as well as for three different time periods: all investigated sessions between 2012 and 2014, the first half of the period from 2012 to mid-2013, and the period with increased observing effort of southern stations after mid-2013. The results of the latter two are visualised in Figs. 3 and 4.

It is clearly evident in Fig. 3 that in the first half of the investigated period southern baselines are less precisely determined in terms of their length WRMS than northern baselines. For medium (6000 km) and long baselines (10,000 km) this difference is 7 mm in WRMS (Table 3). On the other hand, the inequality of the two hemispheres has almost vanished in the sessions after mid-2013

(Fig. 3, right), showing good accordance between all three sets of baselines, southern, northern and mixed ones.

In Fig. 4 the comparison between the two time periods is done for the three sets of baselines, allowing for a more detailed insight into the comparison of specific baselines. We find that baseline length repeatabilities were improved for almost all southern baselines, with only four exceptions. These are, in order with increasing length of the baseline, Tc–Ft (16–17 mm), Tc–Hb (25–30 mm), Tc–Ke (35–40 mm), and the baseline Hb–Ft whose WRMS increased from 29 mm to 32 mm in the later period. Three of these baselines include the station Tc, which, according to Table 1, has contributed to much less sessions in the later period (77 sessions) than before (147 sessions). Main improvements are found for the medium length baselines (6000–10,000 km), which are mostly baselines between Africa (Ht, Hh) and Australia (Hb, Ke, Yg).

For the northern baselines, the results of some individual baselines do change significantly but the total trend does not change much. Although, a small degradation of 1–2 mm in WRMS is found for the more recent sessions. This could be the result of a particularly bad performance of a few baselines in the second half of the period (as visible in Fig. 4, right), or is due to the generally lower number of scans and observations per session for the northern stations in the second period (Table 1).

Also the results for the mixed north–south baselines do not change significantly between the two investigated time periods, at least concerning the trend over all baselines. Studying the individual baselines, for both time periods we find a couple of outliers showing a bit higher WRMS values than the rest of the baselines. For the 2012/13 period these are baselines to Australian stations (Zc–Yg, Ke–Mc, Ke–Sv), while in the 2013/14 period the results for those three baselines could be improved and we find worse results for the baselines Zc–Tc, Sv–Tc, Bd–Tc, and Mc–Hb. As mentioned above, this could be due to the reduced number of sessions with Tc. This is also true for the station Mc, that only contributed to 13 sessions after mid-2013 while it had 24 sessions in the first period.

While the observed improvements for the southern baselines is significant, the reasons for them could be manifold. The simplest conclusion is that by increasing the participation of the southern (AuScope) antennas, we achieve better results. The questions remaining are whether this is purely due to the new schedules with the increased number of scans and observations mainly determined through antenna availability, geography and antenna characteristics, or whether the actual performance of the measurements themselves is decisive. The latter one is influenced by factors like the station's local hardware and antenna capabilities like cabling, the cooling system, etc. but also by the local weather conditions. Troposphere is the major source of error in present day geodetic VLBI. For example, Nilsson and Haas (2010) showed that different levels of tropospheric turbulence as measured at different stations during observations have a direct impact on the results for

Table 3  
WRMS of baseline lengths determined for the investigated R1 and R4 sessions. Values are given for three baseline lengths and we distinguish between southern (SS), mixed (NS), and northern (NN) baselines. Further the comparison is done between the results for the full set of sessions between 2012 and 2014 and the two sets of sessions before/after mid-2013.

	2012–2014	2012–2013/6	2013/7–2014
WRMS	$2/6/10 \cdot 10^3$ km	$2/6/10 \cdot 10^3$ km	$2/6/10 \cdot 10^3$ km
<i>Real observations</i>			
SS	8/15/26 mm	9/18/28 mm	8/12/23 mm
NS	–/16/23 mm	–/16/23 mm	–/16/23 mm
NN	7/13/24 mm	6/11/21 mm	7/12/23 mm
<i>Simulations</i>			
SS	6/14/25 mm	6/16/26 mm	5/14/24 mm
NS	–/13/22 mm	–/15/24 mm	–/13/21 mm
NN	4/10/18 mm	4/10/17 mm	4/10/18 mm

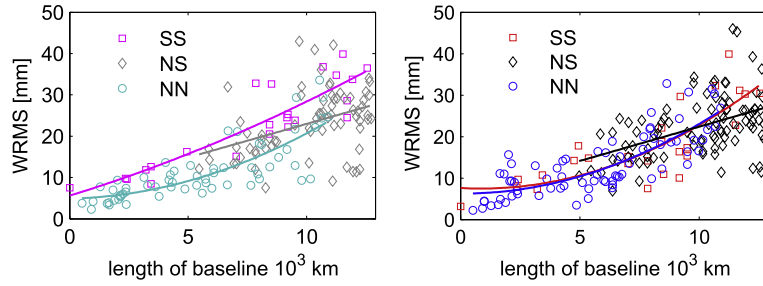


Fig. 3. Baseline length repeatabilities (WRMS) for two time periods of R1 and R4 sessions, 2012–2013/6 (left) and 2013/7–2014 (right). Southern baselines (SS) are marked with squares, north–south baselines (NS) with diamonds, and completely northern baselines (NN) with circles. The lines are quadratic (linear for NS baselines) fits for each set of baselines.

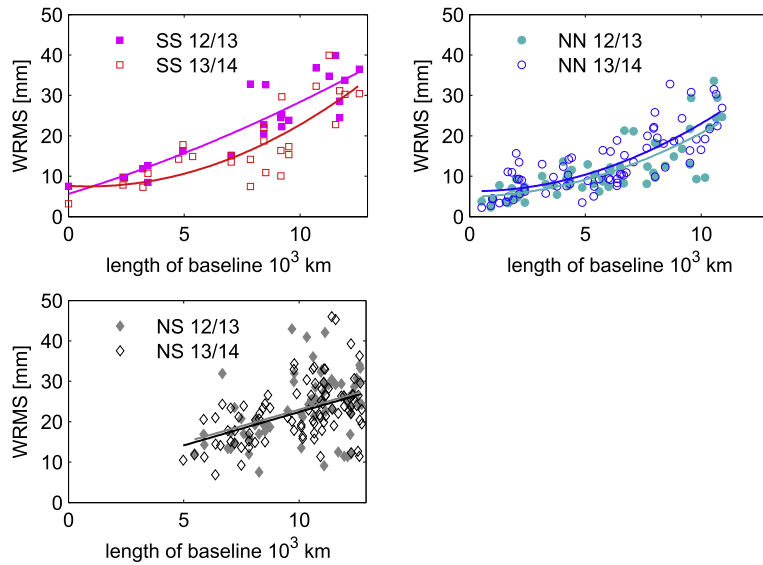


Fig. 4. Baseline length repeatabilities (WRMS) of southern (SS), northern (NN) and mixed (NS) baselines, comparing two time periods of R1 R4 sessions, before (filled symbols) and after (empty symbols) mid-2013. Results are given for each individual baseline, and for better visibility a quadratic (linear in case of the mixed baselines) trend is fitted to the data.

each station. For our analysis, we used the measurement error, as determined during the correlation and fringe fitting procedure, for weighting of the individual observations in the solution.

To investigate the sole effect of the observation plan, independently from globally different tropospheric conditions or actual performance of the measurements, we turn to simulations.

### 3. Simulations

#### 3.1. Simulated baseline length repeatabilities

The simulations were performed with the observation schedules from the 2012–2014 R1 and R4 sessions described above using the VieVS simulator. In the simulated observations we account for the three most important stochastic error sources, namely the wet troposphere, station clocks, and measurement error (Petrachenko et al., 2009; Pany et al., 2010). In order to assess the sole effects of improved station networks and schedules, we assumed

identical conditions at all stations. Tropospheric turbulence was simulated following Nilsson et al. (2007). We used initial zenith wet delays of 150 mm, a structure constant of a turbulent troposphere of  $1.5 \times 10^{-7} \text{ m}^{1/3}$ , an effective height of the troposphere of 2 km, and wind speeds of 0 m/s in the northern direction and 8 m/s in the eastern direction. The height increment for integration was set to 200 m and a correlation interval of 8 h was used. For the clocks an Allan standard deviation of  $1 \times 10^{-14}$  at 50 min was assumed. The measurement error was modeled as white noise per baseline observation with 30 ps standard deviation. In Monte Carlo simulations, each session was simulated 30 times, using new values for zenith wet delays, clocks, and white noise for each repetition. In the subsequent analysis, all observations were weighted equally and baseline lengths repeatabilities were derived for the full set of  $30 \times 302$  sessions.

The results of the simulations are shown in Fig. 5 and Table 3. Comparing the simulations to the results of the real observations, we find good agreement for the southern baselines, while the simulations are somewhat optimistic

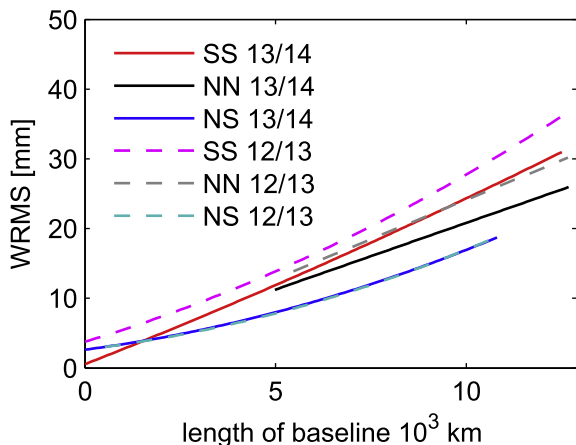


Fig. 5. Simulated baseline length repeatabilities (WRMS) of the 2012–2013/6 (dashed) and the 2013/7–2014 (solid lines) R1 and R4 sessions. We distinguish between southern baselines (SS) north–south baselines (NS) and completely northern baselines (NN). For clarity, only the fits for each set of baselines are shown.

for the northern and mixed baselines. As the simulations are intended to serve as a comparison for the different sets of sessions rather than mimic the real data, this is not a problem for our investigations. The simulations show that, without consideration of different tropospheric conditions or actual measurement performance, the second half of the schedules after mid-2013 (with a larger contribution from southern stations) gives improved repeatabilities for southern baselines. This is also visible in the real observations, although the real observations show an even higher improvement for the medium-length African Australian baselines, what is not visible in the simulations. This indicates that the clear improvement for these southern baselines is also due to other factors. Comparing the results of the two time periods, the simulations also show that the addition of more southern stations does not change the results of fully northern baselines. As the number of scans and observations did not change for northern stations, this is what we expect. However, the observations do show a slight degradation for the more recent sessions. We speculate that this is due to some new stations that were only recently added to the network. Their lower number of baseline observations show worse WRMS and influence the overall statistics. This might also be the reason why we do not see any improvement of the mixed baselines in the observations as we expected it from the simulations. However, the fact that mixed baselines are also improved in the simulations is particularly interesting, as the number of observations for the mixed baselines did not change much (see Fig. 2).

We can conclude that in the simulations a clear difference between the southern and northern baselines persists even for the more recent sessions, while the results of actual observations (Fig. 3) do not show such a difference for the sessions after mid-2013. This proves that there are certainly more factors involved that influence the results in baseline WRMS than solely the observing schedules assuming

identical conditions and performance at all stations. A thorough investigation of these is subject of future studies. As a first step one could strive to better tune the simulations, in a way that they better reflect the actual observations. For example, site-dependent tropospheric conditions as well as clock parameters and measurement noise could be assumed rather than identical assumptions for all stations. Further, it might be worth to investigate the actual performance of the observations as determined through the quality of the correlated observables.

### 3.2. Source position uncertainties

Until now, we have assumed zero error in source positions. In this section we investigate the effect of source position errors on the simulated baseline lengths. The source positions and their uncertainties were taken from the ICRF2 catalog (Ma et al., 2009). The position uncertainties of the observed sources are shown in Fig. 6. Most of the sources have uncertainties better than 0.5 mas, while some sources show maximal uncertainties of up to 3 mas in right ascension ( $RA$ ) and 2 mas in declination ( $Dec$ ). As the estimated source positions on the celestial sphere are actually  $Dec$  and  $RA \cdot \cos(Dec)$ , the errors in right ascension are usually larger closer to the poles (see Fig. 6, top). In the following we adopted the formal error on the position estimate  $d$ , as defined in the ICRF2 document (Ma et al., 2009):

$$d = \sqrt{\sigma_{RA \cdot \cos(Dec)}^2 + \sigma_{Dec}^2 + \sigma_{RA \cdot \cos(Dec)} \sigma_{Dec} C} \quad (1)$$

with  $C$  being the correlation between the estimates of  $RA$  and  $Dec$ . This value is also given in the ICRF2 catalog. In Fig. 7 we show the position error  $d$  versus declination. We binned the sources by declination and calculated the

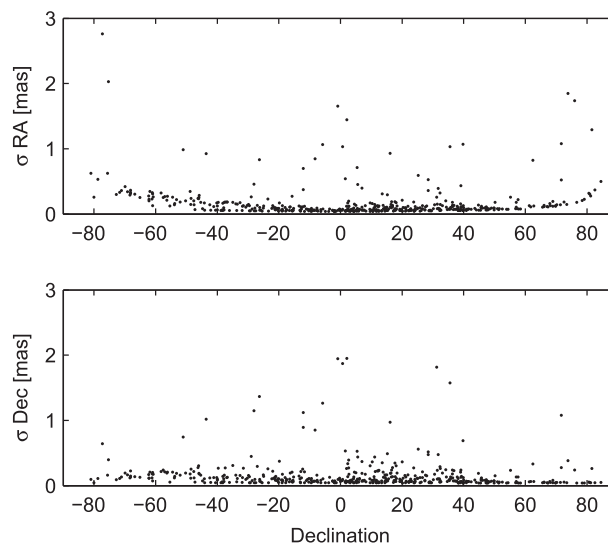


Fig. 6. Formal uncertainties in right ascension (top) and declination (bottom) for the observed sources. Values were taken from the ICRF2 (Ma et al., 2009).

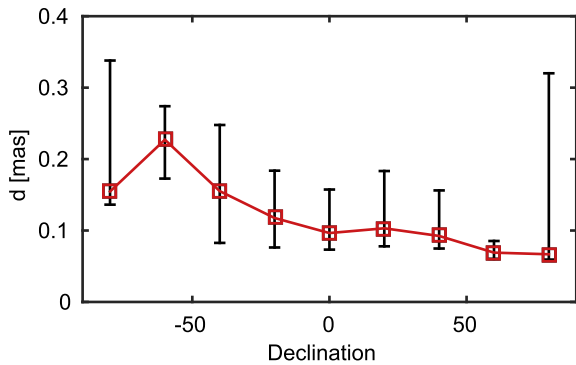


Fig. 7. The dependence of the median position error  $d$  of the observed sources on declination. Sources are binned up by intervals of  $20^\circ$  in declination. The red squares give the medians for each interval, the whiskers indicate the 25th and 75th percentile. (For interpretation of the references to colour in this figure legend, the reader is referred to the web version of this article.)

median values as well as the 25th and 75th percentile for each interval of  $20^\circ$  in declination. It is clearly visible that sources in the south have higher nominal position uncertainties than sources in the north. This result is well known (e.g. Ma et al., 2009).

In the simulations, the source position uncertainties were modeled by randomly shifting the nominal source position ( $RA, Dec$ ) by its uncertainty  $\sigma_{RA, Dec}$  as given in the source catalog.

$$RA = RA + \text{randn} \cdot \sigma_{RA} \text{ and } Dec = Dec + \text{randn} \cdot \sigma_{Dec} \quad (2)$$

The whole set of three years of IVS R-sessions was simulated 30 times, each repetition moving the sources using new random numbers (randn) drawn from a normal distribution with a mean of zero and a standard deviation of 1. One set of source positions was used for all 302 sessions before using a new random number. We ran source position uncertainty-only simulations, where all other stochastic error sources were set to zero.

In the following analysis, source coordinates were fixed and one set of station positions was estimated for each session, applying a no-net-translation and a no-net-rotation condition on all participating antennas. All other parameters were estimated with default settings, as described above.

In Table 4 the effect of simulated errors due to source position uncertainties on baseline lengths repeatabilities are shown. We find that errors in the source positions can affect longer baselines (10,000 km) by up to 10 mm. We find clear differences between southern, mixed, and northern baselines. Besides larger source position errors for southern sources, this is likely due to the fact that the southern baselines are less often observed than the northern ones. Comparing the two time periods, we can see slightly diminished effects for the second set of sessions for the southern baselines, where the number of observations has been improved. For northern and mixed

Table 4

Simulated WRMS of baseline lengths due to source position errors determined for the investigated R1 and R4 sessions. Values are given for three baseline lengths and we distinguish between southern, mixed, and northern baselines. Further the comparison is done between the results for the full set of sessions between 2012 and 2014 and the two sets of sessions before/after mid-2013.

	2012–2014	2012–2013/6	2013/7–2014
WRMS	$2/6/10 \cdot 10^3$ km	$2/6/10 \cdot 10^3$ km	$2/6/10 \cdot 10^3$ km
<i>Nominal source position errors</i>			
SS	2/6/11 mm	2/ 6/11 mm	2/5/9 mm
NS	-/6/9 mm	-/ 6/9 mm	-/6/9 mm
NN	1/3/6 mm	1/3/5 mm	1/3/6 mm
<i>Improved source position errors &lt; 50 <math>\mu</math>s</i>			
SS	1/4/7 mm	1/4/7 mm	1/4/7 mm
NS	-/4/7 mm	-/4/7 mm	-/4/7 mm
NN	1/2/5 mm	1/2/4 mm	1/2/5 mm

baselines, no significant differences between the two time periods were found.

### 3.3. Improved source position uncertainties

In the final investigation of our study we tested whether improved source uncertainties would diminish the simulated effects on baseline length WRMS.

At first we investigated the influence of some particularly bad sources on our simulation. Studying the nominal source position uncertainties for the observed sources, we find 30 sources with  $d > 0.5$  mas. All of these sources were observed in less than 13 sessions. Setting the nominal source position uncertainties of these 30 sources to 0.5 mas and repeating the simulations above showed no significant effects on the results.

Next we simulated a considerably improved ICRF, i.e. all source uncertainties ( $\sigma_{RA}, \sigma_{Dec}$ ) were reduced to be better than or exactly  $50 \mu$ s, which is close to the nominal ICRF2 noise floor of  $40 \mu$ s. Assuming that a source position is determined at the level of about  $500 \mu$ s ( $\sigma_{1\text{sess}}$ ) in one session, all sources would have to be observed in  $N = 100$  sessions to reach this target level ( $\sigma = \sigma_{1\text{sess}}/\sqrt{N}$ ). At present, the nominal source position error  $d$  is highly correlated with the number of sessions a source has been observed in. Fig. 8 shows this relation for the sources that were observed in our investigated sessions. The nominal source position offset as well as the number of observed sessions were taken from the ICRF2 catalog (Ma et al., 2009).

Repeating the simulations with the improved source position errors, the results improved by up to 30% or 8 mm in quadrature for the long southern baselines (Table 4). In Fig. 9 the results of the simulations using the nominal source position errors and those using the improved errors are compared.

## 4. Summary and conclusions

The IVS conducts global VLBI rapid-turnaround experiments twice a week, which are a major input to timely

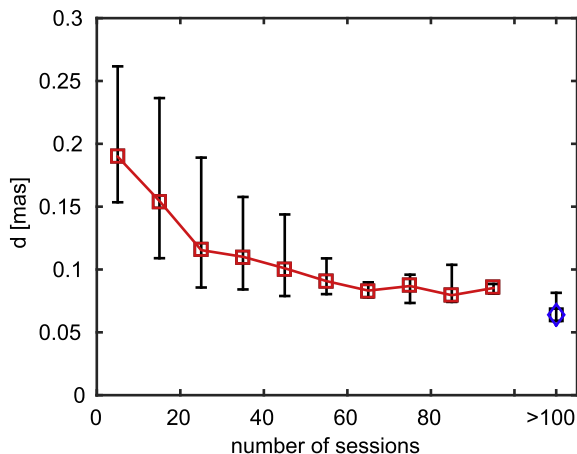


Fig. 8. Nominal source position offset  $d$  versus the number of observed sessions for each source as given in the ICRF2 document. We binned the sources by the number of observed sessions, into bins of 10 sessions. The most right marker (blue) represents all sources that were observed in more than 100 sessions at the time the ICRF2 was generated. The red squares (blue diamond) give the medians for each interval, the whiskers indicate the 25th and 75th percentile. (For interpretation of the references to colour in this figure legend, the reader is referred to the web version of this article.)

EOP time series and future realisations of terrestrial and celestial reference frames. The distribution of the contributing VLBI stations is imbalanced with on average five northern and four southern stations participating in each session. As a result, stations in the southern hemisphere have less scans and less observations per session than stations in the north. Analysing three years of R1 and R4 experiments, we find that before mid-2013 southern baselines are significantly less precisely determined in WRMS of baseline lengths than northern baselines, while in the second period all baselines show the same repeatabilities. This proves that the increased observing effort of southern stations including the Australian AuScope VLBI array since mid-2013 has helped to overcome a previously significant inhomogeneity in the results of the two hemispheres.

In simulations free of non-stochastic station-specific error sources that might be present in the actual observations, we confirmed a difference between the hemispheres for the first period, identifying the observing plan with a lower number of observations and scans as being responsible for the better performance of the northern baselines compared to the north–south and fully southern baselines. However, the improvement in the simulated results is less clear than in real observations. The simulations also show that the imbalance between northern and southern baselines persists also in the more recent schedules. This indicates that the actual performance is also dependent of other factors, as for example the real tropospheric conditions at a particular station or the actual quality of the observations.

Motivated by the fact that the nominal formal uncertainties of source positions are higher for sources in the south than sources in the north, we simulated the effect of source position uncertainties on the baseline length repeatabilities. Applying only source position uncertainties (from ICRF2) in simulations, the baseline length WRMS were about 10 mm for long southern baselines and about 5 mm for long northern baselines. Alternatively, we found that in present-day networks an improved ICRF2 through reduced source uncertainties of  $\leq 50 \mu\text{as}$  could diminish the effect of source uncertainties on baseline length repeatabilities by up to 30% for the long southern baselines. The fact that in the more recent schedules there are more observations to southern sources could help here.

Overall, the presented work confirms that the accuracy of derived baseline lengths during a VLBI session is strongly related to the scheduling and antenna availability. With the recently new southern stations and their increased observing efforts a clear disadvantage for southern baselines could be removed. We can conclude that for present-day networks, with about 10 antennas contributing to a IVS R-session, the north–south imbalance can be overcome as long as the in total fewer southern stations participate in more sessions than the in total more northern stations.

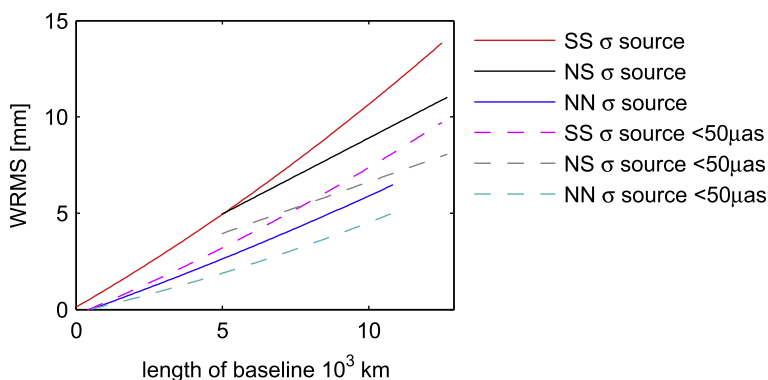


Fig. 9. Simulated WRMS of session-wise estimated baseline lengths due to source position errors. We distinguish between fully southern baselines with both antennas located in the southern hemisphere (SS), fully northern baselines (NN), and mixed baselines (NS). For clarity, only the fits for each set of baselines are shown. The solid lines give the results for the nominal source position errors while the dashed lines are the results of using improved source position errors of  $\leq 50 \mu\text{as}$ .

## Acknowledgements

We wish to thank the International VLBI Service for Geodesy and Astrometry (IVS) for access to VLBI data used in this paper. Parts of the data were collected through the AuScope Initiative, funded under the National Collaborative Research Infrastructure Strategy (NCRIS), an Australian Commonwealth Government Programme. LP and SSS were supported by the Australian Research Council (FS1000100037 and DE130101399). We kindly thank three anonymous reviewers for great suggestions how to improve this investigation.

## References

- Altamimi, Z., Collilieux, X., Métivier, L., 2011. ITRF2008: an improved solution of the international terrestrial reference frame. *J. Geod.* 85 (8), 457–473.
- Böhm, J., Böhm, S., Nilsson, T., Pany, A., Plank, L., Spicakova, H., Teke, K., Schuh, H., 2012. The new vienna VLBI software VieVS. In: Proceedings of the 2009 IAG Symposium, Buenos Aires, Argentina, International Association of Geodesy Symposia, vol. 136, 31 August–4 September, 2009.
- Gipson, J. (Ed.), 2012. Sked: VLBI Scheduling Software. Program Reference Manual, Goddard Space Flight Center.
- Krásná, H., Böhm, J., Plank, L., Nilsson, T., Schuh, H., 2014. Atmospheric effects on VLBI-derived terrestrial and celestial reference frames. In: Rizos, C., Willis, P. (Eds.), IAG Symp. 139. Earth in the Edge: Science for a Sustainable Planet, pp. 203–207.
- Lovell, J., McCallum, J., Reid, P., McCulloch, P., Baynes, B., Dickey, J., Shabala, S., Watson, C., Titov, O., Ruddick, R., Twilley, R., Reynolds, C., Tingay, S., Shield, P., Adada, R., Ellingsen, S., Morgan, J., Bignall, H., 2013. The AuScope geodetic VLBI array. *J. Geod.* 87, 527–538.
- Ma, C., Arias, E., Bianco, G., Boboltz, D., Bolotin, S., Charlot, P., Engelhardt, G., Fey, A., Gaume, R., Gontier, A.M., Heinkelmann, R., Jacobs, C., Kurdubov, S., Lambert, S., Malkin, Z., Nothnagel, A., Petrov, L., Skurikhina, E., Sokolova, J., Souchay, J., Sovers, O., Tesmer, V., Titov, O., Wang, G., Zharov, V., Barache, C., Böckmann, S., Collioud, A., Gipson, J., Gordon, D., Lytvyn, S., MacMillan, D., Ojha, R., 2009. The second realization of the international celestial reference frame by very long baseline interferometry. In: IERS Technical Note 35, Frankfurt am Main: Verlag des Bundesamts für Kartographie und Geodäsie. Presented on behalf of the IERS/IVS Working Group.
- MacMillan, D., Ma, C., 1994. Evaluation of very long baseline interferometry atmospheric modeling improvements. *J. Geophys. Res.* 99 (B1), 637–651.
- MacMillan, D., Ma, C., 2007. Radio source instability in VLBI analysis. *J. Geod.* 81, 443–453.
- Nilsson, T., Haas, R., 2010. Impact of atmospheric turbulence on geodetic very long baseline interferometry. *J. Geophys. Res.* 115, B03407. <http://dx.doi.org/10.1029/2009JB006579>.
- Nilsson, T., Haas, R., Elgered, G., 2007. Simulations of atmospheric path delays using turbulence models, in: Böhm, J., Pany, A., Schuh, H. (Eds.), Proceedings of the 18th European VLBI for Geodesy and Astrometry Working Meeting, 12–13 April 2007, Vienna, vol. 79, pp. 175–180. Schriftenreihe der Studienrichtung Vermessung und Geoinformation, Technische Universität Wien, ISSN 1811-8380.
- Nilsson, T., Böhm, J., Schindelegger, M., Schuh, H., 2012. High Frequency earth rotation parameters estimated from the CONT campaigns, in: Behrend, D., Baver, K. (Eds.), International VLBI Service for Geodesy and Astrometry 2012 General Meeting Proceedings, pp. 390–394. NASA/CP-2012-217504, <http://ivscc.gsfc.nasa.gov/publications/gm2012/nilsson.pdf>
- Pany, A., Böhm, J., MacMillan, D.S., Schuh, H., Nilsson, T., Wresnik, J., 2010. Monte Carlo simulations of the impact of troposphere, clock and measurement errors on the repeatability of VLBI positions. *J. Geod.* 85 (1), 39–50.
- Petit, G., Luzum, B. (Eds.), 2010. IERS Conventions 2010, Frankfurt am Main: Verlag des Bundesamts für Kartographie und Geodäsie. IERS Technical Note No. 36.
- Petrachenko, B., Niell, A., Behrend, D., Corey, B., Böhm, J., Charlot, P., Collioud, A., Gipson, J., Haas, R., Hobiger, T., Koyama, Y., MacMillan, D., Malkin, Z., Nilsson, T., Pany, A., Tuccari, G., Whitney, A., Wresnik, J., 2009. Progress Report of the IVS VLBI2010 Committee: Design Aspects of the VLBI2010 System. NASA/TM-2009-214180. <ftp://ivscc.gsfc.nasa.gov/pub/misc/V2C/TM-2009-214180.pdf>.
- Petrov, L., Gordon, D., Gipson, J., MacMillan, D., Ma, C., Fomalont, E., Craig Walker, R., Carabajal, C., 2009. Precise geodesy with the very long baseline array. *J. Geod.* 83 (9), 859–876. <http://dx.doi.org/10.1007/s00190-009-0304-7>.
- Schuh, H., Behrend, D., 2012. VLBI: a fascinating technique for geodesy and astrometry. *J. Geodyn.* 61, 68–80.
- Schuh, H., Böhm, J., 2013. Very long baseline interferometry for geodesy and astrometry. In: Xu, G. (Ed.), Sciences of Geodesy – II. Springer-Verlag, Berlin Heidelberg. <http://dx.doi.org/10.1007/978-3-642-28000-9-7>.
- Sun, J., Böhm, J., Nilsson, T., Krásná, H., Böhm, S., Schuh, H., 2014. New VLBI2010 scheduling strategies and implications on the terrestrial reference frames. *J. Geod.* 88, 449–461.
- Titov, O., 2007. Effect of the selection of reference radio sources on geodetic estimates from VLBI observations. *J. Geod.* 81, 455–468. <http://dx.doi.org/10.1007/s00190-007-0145-1>.
- Titov, O., 2009. A new estimator for VLBI baseline length repeatabilities. *J. Geod.* 83, 1041–1049. <http://dx.doi.org/10.1007/s00190-009-0322-5>.
- Wijaya, D., Böhm, J., Karbon, M., Krásná, H., Schuh, H., 2013. Atmospheric pressure loading, in: Böhm, J., Schuh, H. (Eds.), Atmospheric Effects in Space Geodesy, pp. 137–158, ISBN 978-3-642-36931-5.